

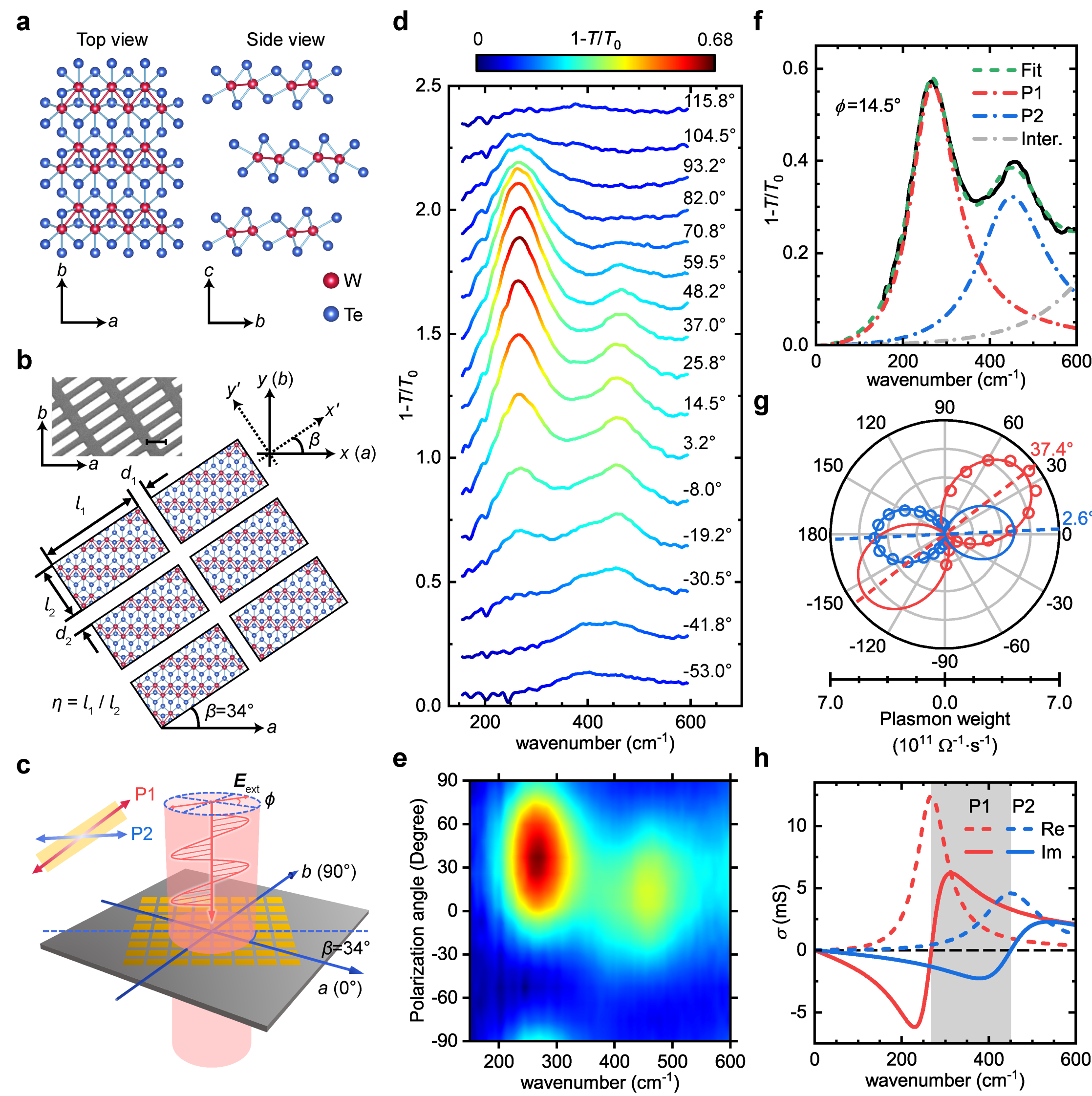
## Abstract

Hyperbolic shear modes enable extreme optical confinement and directional propagation, but their implementation remains challenging. Natural materials offer limited design flexibility, while artificial twist-based structures rely on interlayer coupling that is acutely sensitive to thickness mismatch, interface contamination, twist-angle inhomogeneity, and lattice strain, resulting in degraded shear performance.

Here we establish a single-sheet-integrated paradigm for hyperbolic shear metasurfaces based on Td-WTe<sub>2</sub> skew-rectangle arrays. These low-symmetry plasmonic resonators support detuned, non-orthogonal dual localized surface plasmon resonances in the far-infrared range. Polarization-resolved Fourier transform infrared spectroscopy confirms the coexistence of two geometrically controlled resonances with polarization axes spanning a 140° tuning range. The emergence of hyperbolic shear surface waves exhibiting both axial dispersion and loss redistribution is collectively confirmed by finite-element simulations of surface waves, analytical isofrequency contours derived from Maxwell's equations, and random phase approximation calculations. We further reveal that the shear phenomenon arises from the superposition of intrinsic crystalline anisotropy and extrinsic geometric anisotropy.

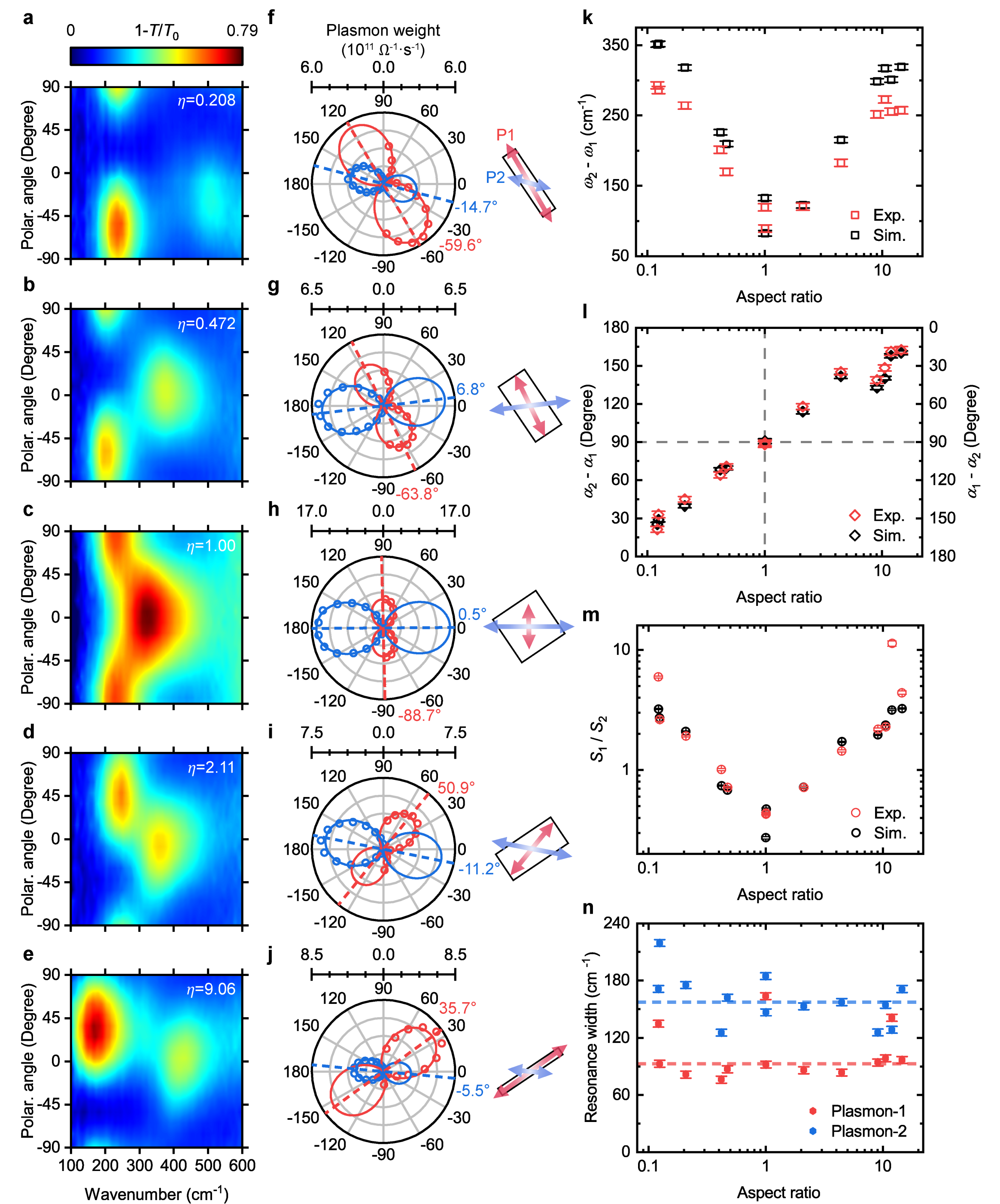
By integrating dual resonances within a single patterned sheet, this approach ensures intrinsic mode coupling with guaranteed robustness, and more importantly, enables independent tuning through multiple geometric degrees of freedom. Our study establishes a universal design platform for hyperbolic shear nanophotonics, which readily extends to diverse anisotropic plasmonic materials.

## Optical characterization of HShMs



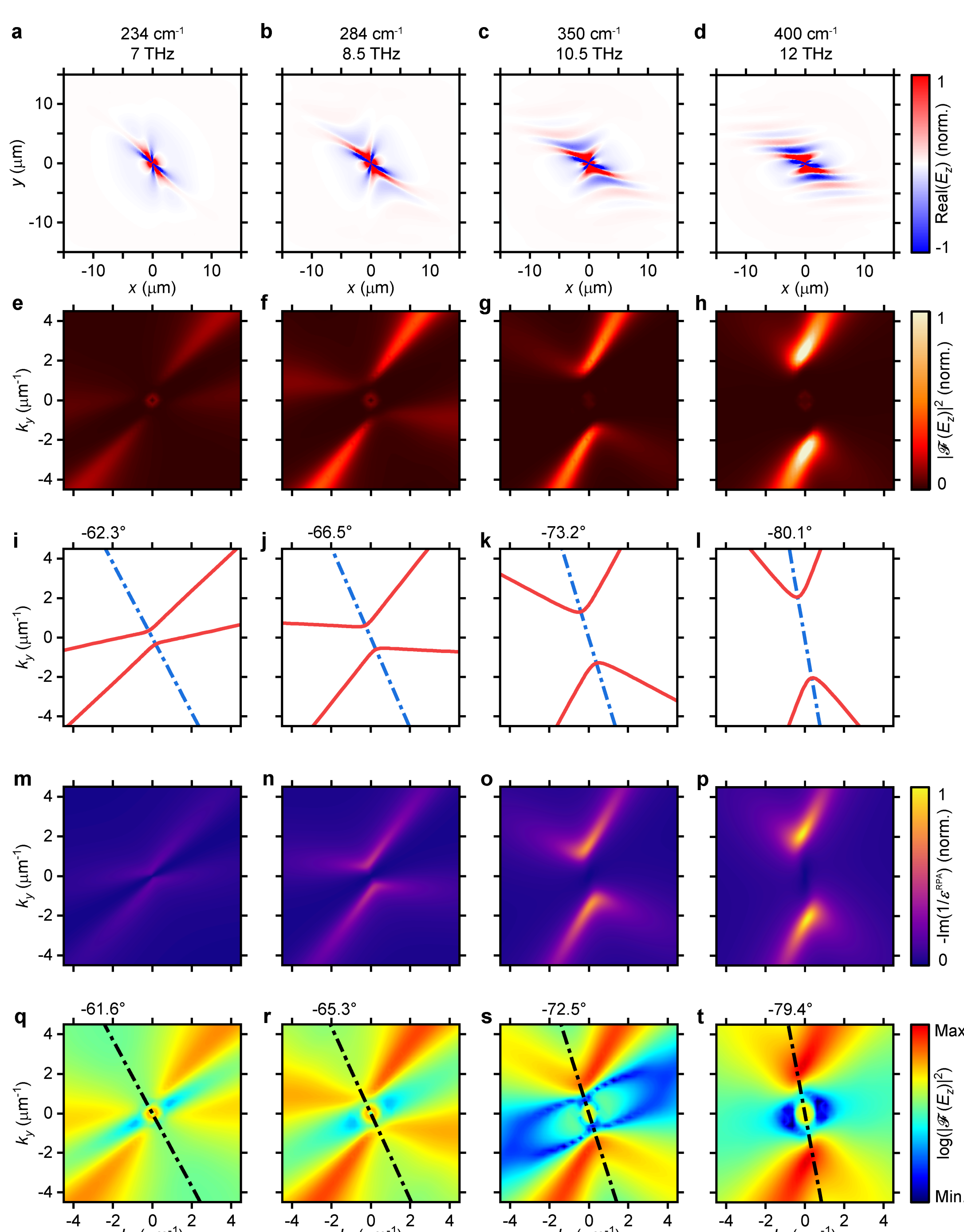
**a** Illustration of the Td-WTe<sub>2</sub> crystal structure. **b** Schematic of the skew-rectangle array patterned from a single-crystal sheet. Top-left inset: SEM image; scale bar, 2 μm. **(d–h)** show measurements on this sample. Top-right inset: Definitions coordinate systems. **c** Illustration of far-field measurement; top-left inset shows a schematic of the single skew-rectangle with plasmon polarization directions indicated. **d** Polarization-dependent far-IR extinction spectra of the sample shown in the inset of **(b)**. **e** The corresponding pseudocolor map of **(d)**. **f** Representative extinction spectrum with fitted curves. **g** Polarization dependence of plasmon weights. Solid lines show fits. **h** Sheet optical conductivities projected along the respective plasmon polarization directions.

## Geometric control of HShMs



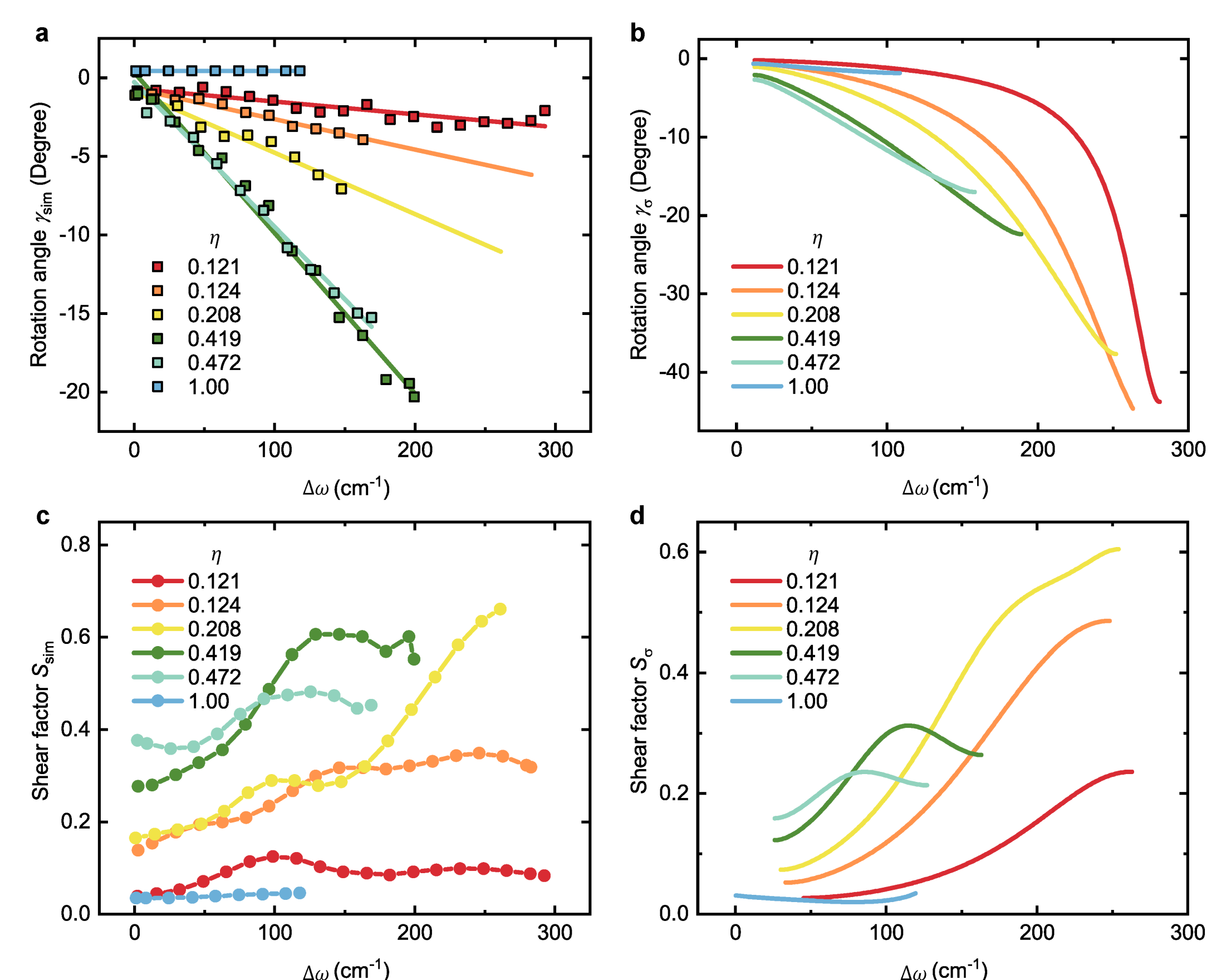
**a–e** Representative pseudocolor maps of experimental extinction spectra for skew-rectangle arrays with different aspect ratios. **f–j** Polar plots of plasmon weights corresponding to **(a–e)**. Right insets: schematics of the corresponding skew-rectangles with indicated polarization directions. **k** Frequency separation between the two plasmon resonances versus aspect ratio (logarithmic scale). **l** Relative angle between the plasmon polarization directions plotted against aspect ratio (logarithmic scale). A vertical dashed line marks  $\eta = 1$ , and a horizontal dashed line marks 90°. **m** Ratio of plasmon weights versus aspect ratio, with both axes on logarithmic scales, comparing experimental and simulated results. **n** Resonance widths versus aspect ratio (logarithmic scale), showing experimental data. Horizontal dashed lines indicate the median values for each plasmon.

## Characterization of hyperbolic shear surface waves



**a–d** Real-space electric field distributions obtained from finite-element simulations of surface waves. **e–h** Momentum-space intensity distributions obtained by Fourier transforming the real-space fields shown in **(a–d)**. **i–l** Isofrequency contours of surface modes obtained from analytical solutions of Maxwell's equations. **m–p** Momentum-space mode strength distributions calculated using RPA. **q–t** Logarithmic-scale momentum-space intensity distributions derived from **(e–h)**.

## Aspect-ratio-dependent hyperbolic shear parameters



**a** Optical principal axis rotation angle  $\gamma_{\text{sim}}$  extracted from finite-element simulations of surface waves (squares). Linear fits (lines) are shown, some extending across the hyperbolic range. **b** Optical principal axis rotation angle  $\gamma_{\sigma}$  calculated from the diagonalization of the imaginary part of the sheet conductivity tensor. **c** Shear factor  $S_{\text{sim}}$  determined from the normalized intensity contrast between adjacent quadrants in momentum space (based on finite-element simulations of the type shown in Fig. 3e–h), using the optical principal axes identified in **(a)**. Circles represent simulation data; lines are guides to the eye. **d** Shear factor  $S_{\sigma}$  derived from the off-diagonal elements of the real part of the conductivity tensor after diagonalization of its imaginary part.